Chapter 2
Nanomechanical Characterization of Lead Free Solder Joints

Md Hasnine, Muhannad Mustafa, Jeffrey C. Suhling, Barton C. Prorok, Michael J. Bozack, and Pradeep Lall

Abstract The mechanical properties of a lead free solder are strongly influenced by its microstructure, which is controlled by its thermal history including solidification rate and thermal aging after solidification. In our ongoing research, we are exploring aging effects in lead free solder joints, and correlating the results to measured behavior from miniature bulk tensile samples. As a part of these efforts, the mechanical properties and creep behavior of lead free solders are being characterized by nano-mechanical testing of single SAC305 solder joints extracted from PBGA assemblies. Using nanoindentation techniques, the stress–strain and creep behavior of the SAC solder materials have been explored at the joint scale. Mechanical properties characterized included the elastic modulus, hardness, and yield stress. The test results show that the mechanical properties (modulus, hardness) of single grain SAC305 joints were dependent on the crystal orientation. Using a constant force at max indentation, the creep response of the solder joint materials has also been measured as a function of the applied stress level. An approach has been developed to estimate tensile creep strain rates for low stress levels using nanoindentation creep data measured at very high compressive stress levels.

Keywords Nanoindentation • Lead free solder • SAC alloy • Modulus • Hardness • Creep

2.1 Introduction

The ongoing transition to lead free soldering has been motivated by environmental concerns, legislative mandates, and market differentiation. Although no clear solution has been identified for all applications; Sn-Ag, Sn-Ag-Cu (SAC), and other alloys involving elements such as Sn, Ag, Cu, Bi, In, and Zn have been identified as potential replacements for standard 63Sn-37Pb eutectic solder. Several SAC alloys, such as 96.5Sn-3.0Ag-0.5Cu (SAC305), 95.5Sn-3.8Ag-0.7Cu (SAC387), 95.5Sn-3.9Ag-0.6Cu (SAC396) and 95.5Sn-4.0Ag-0.5Cu (SAC405), have been the proposed by various user groups and industry experts. For enhanced reliability of portable electronic devices during shock/drop loading (e.g. high strain rates), SAC alloys with low silver content have been recommended including 98.5Sn-1.0Ag-0.5Cu (SAC105). The main benefits of the various SAC alloy systems are their relatively low melting temperatures compared with the Sn-Ag binary eutectic alloy, as well as their higher strength, superior resistance to creep and thermal fatigue and solderability when compared to other lead free solders.

Solder joint fatigue is one of the predominant failure mechanisms in lead free electronic assemblies exposed to thermal cycling. Thus, accurate mechanical properties and constitutive equations for solder materials are needed for use in mechanical design, reliability assessment, and process optimization. Ma et al. [1] have reviewed the literature on the mechanical behavior of lead free solders. The mechanical properties of a lead free solder are strongly influenced by its microstructure, which is controlled by its thermal history including solidification rate and thermal aging after solidification. Due to aging phenomena, the microstructure, mechanical response, and failure behavior of lead free solder joints in electronic assemblies are constantly evolving when exposed to isothermal aging and/or thermal cycling environments.

Md. Hasnine • M. Mustafa • J.C. Suhling (✉) • B.C. Prorok • M.J. Bozack • P. Lall
Department of Mechanical Engineering, and Center for Advanced Vehicle and Extreme Environment Electronics (CAVE^3), Auburn University, Auburn, AL 36849, USA
e-mail: jsuhling@auburn.edu

G. Shaw III et al. (eds.), *MEMS and Nanotechnology, Volume 5: Proceedings of the 2013 Annual Conference on Experimental and Applied Mechanics*, Conference Proceedings of the Society for Experimental Mechanics Series,
DOI 10.1007/978-3-319-00780-9_2,

Such aging effects are greatly exacerbated at higher temperatures typical of thermal cycling qualification tests. However, significant changes occur even with aging at room temperature.

In our prior papers on elevated temperature aging effects [2–9], we have demonstrated that the observed material behavior variations of SACN05 (N = 1, 2, 3, 4) lead free solders during isothermal aging at a variety of elevated temperatures (e.g. 25 C, 50 C, 75 C, 100 C, and 125 C) were unexpectedly large and universally detrimental to reliability. The measured stress–strain data demonstrated large reductions in stiffness, yield stress, ultimate strength, and strain to failure (up to 50 %) during the first 6 months after reflow solidification. After approximately 10–20 days of aging, the lead free solder joint material properties were observed to degrade at a slow but constant rate. In addition, even more dramatic evolution was observed in the creep response of aged solders, where up to 10,000× increases in the secondary creep rates were observed for aging up to 6 months. The aged solder materials were also found to enter the tertiary creep range (imminent failure) at much lower strain levels than virgin solders (non-aged, tested immediately after reflow solidification). In our most recent studies [7, 8], we have investigated the effects of aging on the parameters in the Anand viscoplastic constitutive model and the fatigue life of lead free solders.

All of our prior work has been based on uniaxial testing of miniature bulk solder tensile specimens. These samples were solidified in glass tubes under a controlled temperature profile in an effort to accurately match the microstructure of actual solder joints. Complementary studies by other research groups have verified aging induced degradations of SAC mechanical properties. In those investigations, mechanical testing was performed on a variety of sample geometries including lap shear specimens, Iosipescu shear specimens, and custom solder ball array shear specimens.

There have been limited prior mechanical loading studies on aging effects in actual solder joints extracted from area array assemblies (e.g. PBGA or flip chip) [10–13]. This is due to the extremely small size of the individual joints, and the difficulty in gripping them and applying controlled loadings (tension, compression, or shear). Pang et al. [10] have measured microstructure changes, intermetallic layer growth, and shear strength degradation in custom SAC single ball joint lap shear specimens subjected to elevated temperature aging. Darveaux [11] performed an extensive experimental study on the stress–strain and creep behavior of solder using specially constructed double lap shear specimens with a 10 × 10 area array solder balls. He found that aging for 1 day at 125 C caused significant effects on the stress–strain and creep behavior. For example, aged specimens were found to creep much faster than non-aged specimens by a factor of up to 20 times for both SAC305 and SAC405 solder alloys. Wiese, et al. [12] also studied the effects of aging on solder joint creep using custom assemblies with four flip chip solder balls, and found highly accelerated creep rates after aging at 125 C. Finally, Dutta and coworkers [13] used an impression creep technique with a cylindrical punch to study creep in PBGA solder balls that had been subjected to thermal-mechanical cycling.

Nanoindentation techniques have been widely used to probe the mechanical properties and deformation behavior of extremely small material samples [14]. Over the past decade, it has been applied by several investigators to characterize lead free solder joints and intermetallic compounds (IMC) in lead free solder joints [15–29]. In early studies by Rhee et al. [15, 16], Chromik et al. [17], and Deng and coworkers [18, 19], the elastic modulus E and hardness H of various regions in Sn-Ag and SAC lead free solder joints were explored by nanoindentation. In particular, the properties for the Sn-rich phase (β-tin) and the eutectic phase (containing β-tin and a mix of Sn-Ag and Sn-Cu intermetallics) were explored. Attempts were also made to indent individual Sn-Ag and Sn-Cu intermetallic particles [17–19], and then to compare the properties of the IMCs to those for the solder joint phases. Rhee et al. [15] also measured changes in the mechanical properties after the joints were subjected to thermal-mechanical cycling.

Gao et al. [20, 21] have used nanoindentation to characterize the effects of loading rate on the modulus and hardness of Sn-Ag lead free solders. They also performed creep experiments for two different microstructures (bulk cast and reflowed), and examined the effects of elevated temperature aging on the hardness. Indentation experiments with a heated stage to control the solder sample temperature have been performed by Sun et al. [22], Liu et al. [23], Gao et al. [24], and Han and coworkers [25]. The alloys tested in these studies included SAC387, 80Au-20Sn, SAC305, and SAC357, respectively. In all of these investigations, the temperature dependencies of the mechanical properties (E, H) of the solder matrix or individual solder phases were characterized. In addition, the sensitivity of the creep response of lead free solder to temperature has also been examined [23–25]. Han et al. [26] have studied the indentation size effect on the creep behavior of SAC357 lead free solder.

The effect of thermal aging on the mechanical properties of intermetallic compounds at SAC solder joint interfaces have been explored using nanoindentation by Xu and Pang [27, 28] and Song et al. [29]. Significant drops in both the modulus and hardness were recorded for aged samples relative to non-aged samples. Xu and Pang [27] also characterized the mechanical properties of the various phases and IMCs in a SAC387 solder joint. Venkatadri et al. [30] have studied the effects of aging on lead free solder joints using a micro-hardness test to perform single idents on joints.

As discussed above, there is an extensive literature that documents the large changes in the microstructure and mechanical behavior that occur in bulk lead free solder specimens during isothermal aging. There have also been some

limited investigations on the effects of aging on mechanical properties and creep behavior of solder joint arrays. In addition, nanoindentation has been utilized to study aging induced changes in the mechanical properties of intermetallic compound layers in solder joints. However, there has been little work on aging effects on mechanical properties and creep behavior in individual solder joints. Such knowledge is crucial for the optimizing the design, manufacturing, and reliability of microelectronic packages. Characterization of individual joints is quite challenging because of their extremely small size, and the difficulty in gripping them and applying controlled loadings.

In our ongoing research, we are exploring aging effects in lead free solder joints, and correlating the results to measured behavior from miniature bulk tensile samples. As a part of these efforts, the mechanical properties and creep behavior of lead free solders are being characterized by nano-mechanical testing of single SAC305 solder joints extracted from PBGA assemblies. Using nanoindentation techniques, the stress–strain and creep behavior of the SAC solder materials have been explored at the joint scale. Mechanical properties characterized included the elastic modulus, hardness, and yield stress. The test results show that the mechanical properties (modulus, hardness) of single grain SAC305 joints were highly dependent on the crystal orientation. Using a constant force at max indentation, the creep response of the solder joint materials has also been measured as a function of the applied stress level. An approach has been developed to estimate tensile creep strain rates for low stress levels using nanoindentation creep data measured at very high compressive stress levels.

2.2 Experimental Procedure

2.2.1 Solder Joint Samples

Lead free solder joints were extracted from PBGA assemblies (Amkor CABGA, 14 × 14 mm, 192 balls, 0.8 mm ball pitch, 0.46 mm ball diameter). The test boards were assembled as part of the iNEMI Characterization of Pb-Free Alloy Alternatives Project [31], and a variety of samples with 14 different solder joint alloys are being studied. In this paper, we concentrate on presenting results for SAC305 (96.5Sn-3.0Ag-0.5Cu) solder joints. These joints were extracted from test boards where the original components had SAC305 solder balls, the bare test boards had ENIG surface finish, and where SAC305 solder paste was used in the surface mount assembly process. The assembled PBGA components were cut out from the test boards and then cross-sectioned into samples of four joints each. These samples were mounted in an epoxy molding compound suitable for SEM microscopy, and then polished to a level appropriate for nanoindentation. Details of the sample preparation process include mechanical grinding with several SiC papers (#320 to #400, #600, #800 and #1200), and then final polishing with 1 μm diamond paste followed by 0.05 μm colloidal silica suspensions. This resulted in mirror finish samples suitable for nanoindentation tests and SEM microscopy.

2.2.2 Nanoindentation System and Test Procedures

The nanoindentation tests were conducted using an instrumented MTS Nanoindenter XP system with a Berkovich tip indenter. The load versus indentation displacement normal to the cross-section surface was measured during each indentation experiment, and the elastic modulus could then be extracted using the approach proposed by Oliver and Pharr [32, 33] to process the measured slope of the load–displacement curve in the unloading phase. In addition, the Continuous Stiffness Measurement (CSM) technique [33, 34] was also used in all experiments to extract elastic modulus and hardness as a function of the distance from the surface (indentation depth).

A typical cross-sectioned lead free solder ball sample after nanoindentation testing is shown in Fig. 2.1, and a close-up view of an example permanent indentation mark is shown in Fig. 2.2. For each set of experimental test conditions, an array of several indents spaced 30 μm apart were made (e.g. 2 × 3 array as shown in Fig. 2.1), and the individual indent test values were averaged to obtain statistically relevant results and consistency of inspection. All tests were performed on single grain (Sn crystal) solder balls, so that there were no orientation effects caused by an indentation array covering two or more grain boundaries of grains with significantly different crystal orientation (different material properties).

A maximum load of 30 mN was selected for the tests so that the indentation marks were large enough to cover all the phases of SAC305 solder material (see Fig. 2.2). Thus, the nanoindentation tests characterized the global mechanical

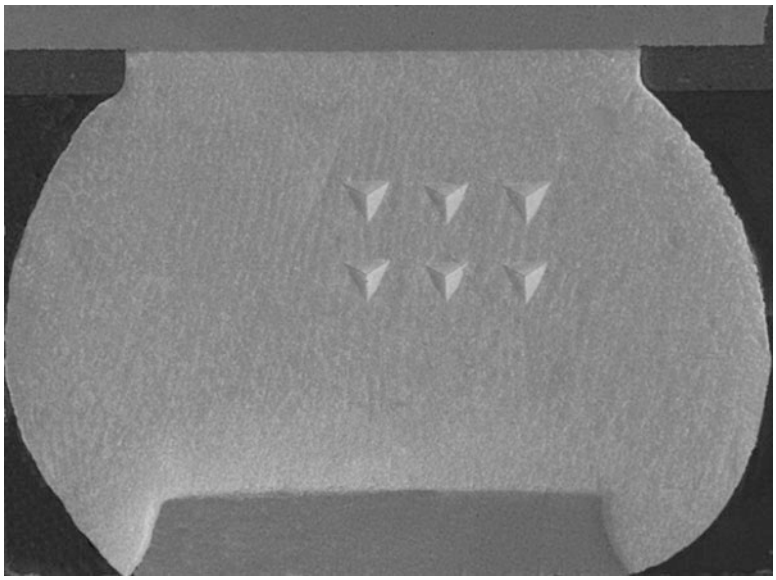

Fig. 2.1 Solder ball after nanoindentation testing

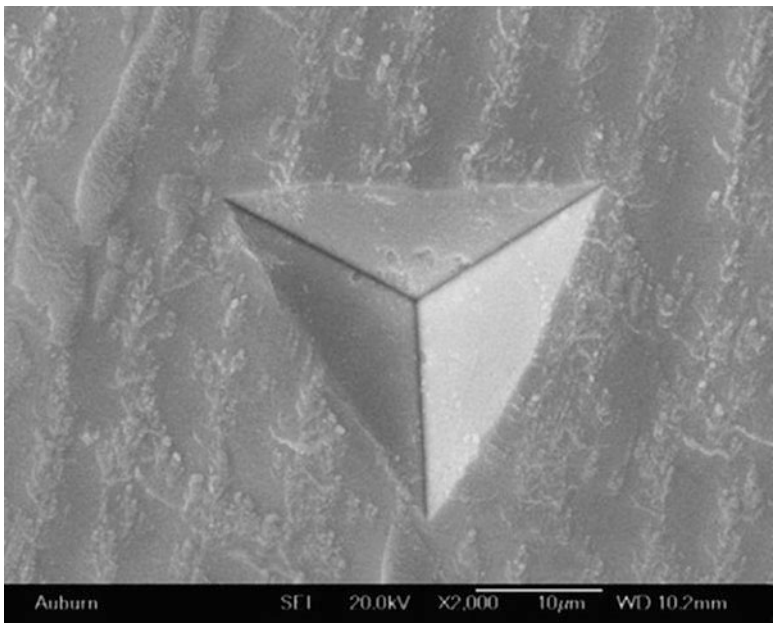

Fig. 2.2 Permanent indentation after testing

properties of the solder joints, rather than the localized properties in the β-Sn phases (Sn-rich dendrites) or in the eutectic phases between dendrites that contain Sn-Ag and Sn-Cu intermetallics. Indentation experiments were conducted at constant indentation displacement rate of 10 nm/s, corresponding to an effective strain rate of 0.05 s^{-1}. Calibration of the load and hardness measurements was performed on fused silica.

Indentation creep tests were performed holding the load constant at its maximum value of 30 mN for 500–1,000 s. After this dwell, the sample was unloaded at the same 10 nm/s displacement rate used during loading. There was also a holding period of 60 s after 90 % unloading to allow for thermal drift correction. In our work, the thermal drifts were kept smaller than 0.05 nm/s, and the thermal drift effects were excluded from the resulting displacement data.

2.3 Indentation Procedure for Lead Free Solder Joints

2.3.1 Measurement of Elastic Modulus and Hardness

A typical nanoindentation load versus displacement (P vs. h) curve for one of the SAC305 solder joint samples is shown in Fig. 2.3. During indentation, continuous load–displacement data are recorded. The measured response consists of three segments: (1) loading at constant deformation rate (10 nm/s) to the indentation force reaches its prescribed maximum value of 30 mN; (2) dwell (creep) for 500 s at maximum load of 30 mN; and (3) unloading at the same constant deformation rate (10 nm/s). The loading curve is a function of loading rate. The slope $S = dP/dh$ of the unloading region at maximum load is called the unloading stiffness, and can be used to calculate the elastic modulus E and hardness H at the point of maximum indentation using the Oliver and Pharr method [32, 33]. In addition to S, the procedures to calculate E and H (see below) require the values of P_{max}, h_{max}, ν (Poisson's ration of the indented material), and several geometrical parameters and materials constants for the indentor tip.

In nanoindentation testing, the hardness (Meyer hardness) H is defined as maximum load divided by projected contact area A of the indentation at maximum load:

$$H = \frac{P_{max}}{A} \tag{2.1}$$

The hardness is thought of as a material flow resistance or resistance to plastic deformation. For many metals, the hardness and yield stress can be related by the approximation

$$H \approx 3\sigma_Y \quad \text{or} \quad \sigma_Y \approx \frac{H}{3} \tag{2.2}$$

This empirical expression is often referred to as the Tabor relationship [35, 36].

For the Berkovich indentor tip used in the work, the projected contact area at maximum load is given by:

$$A = 24.5h_c^2 + Ch_c \tag{2.3}$$

where h_c is the vertical distance in which the contact is made, and C is a geometrical factor that is approximately 150 nm [34]. The distance h_c can be related to the measured indentation displacement using theory of elasticity based contact mechanics:

$$h_c = h_{max} - h_s = h_{max} - \varepsilon\frac{P_{max}}{S} \tag{2.4}$$

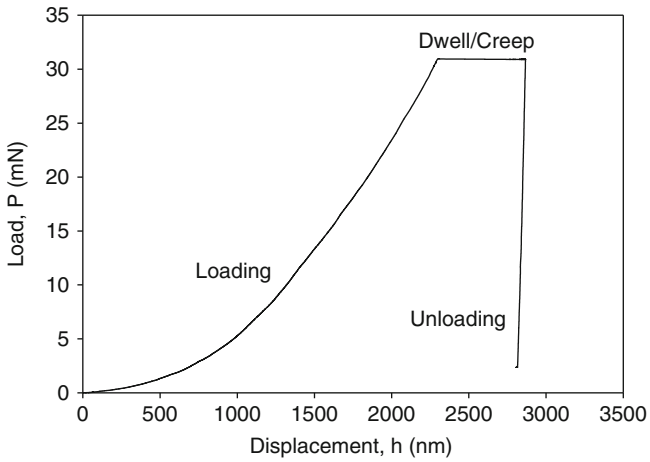

Fig. 2.3 Typical nanoindentation load–displacement curve for a SAC305 solder joint

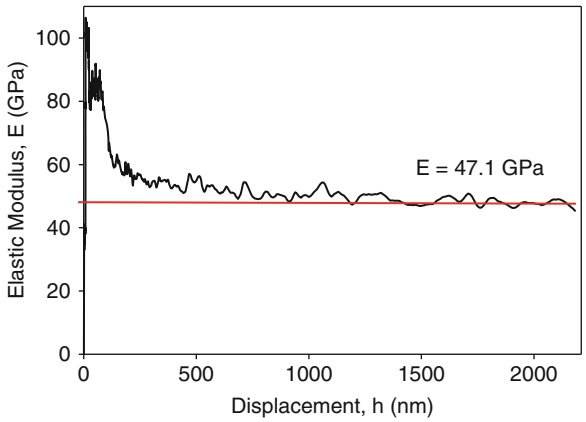

Fig. 2.4 Nanoindentation elastic modulus of SAC305 solder as a function of indentation depth

where h_{max} is the measured maximum indentation displacement from the P vs. h curve, h_s is the displacement of the surface of the material at the perimeter of the indentor contact, and $\varepsilon \approx 0.75$ is a geometrical constant for the Berkovich indentor tip [33]. Combining Eqs. 2.1, 2.2, 2.3 and 2.4, the hardness H and projected contact area A can be related to P_{max}, h_{max}, and S measured from the nanoindentation P vs. h curve. Equation 2.2 can then be used to estimate the yield stress of the indented material from the measured hardness.

Using the assumption that the contact area remains constant during withdrawal of the indentor tip and theory of elasticity solutions for contact of a material with a rigid punch, it can be established that the unloading stiffness from the recorded nanoindentation curve is given by:

$$S = \frac{dP}{dh} = \frac{2\beta\sqrt{A}}{\sqrt{\pi}} E_r \quad \text{or} \quad \frac{1}{E_r} = \frac{2\beta\sqrt{A}}{\sqrt{\pi}\, S} \tag{2.5}$$

where $\beta \approx 1$ is a geometrical factor for the chosen indentor tip and E_r is the reduced modulus [32, 33]. The desired elastic modulus E of the material being indented is related to the reduced modulus using

$$E = \frac{1 - v^2}{\left[\frac{1}{E_r}\right] - \left[\frac{1-v_i^2}{E_i}\right]} \tag{2.6}$$

where v is the Poisson's ratio of the indented material (usually assumed to be 0.3 if unknown), v_i is the known Poisson's ratio of the indentor tip material, and E_i is the known elastic modulus of the indentor tip material [14, 32, 33]. Combining Eqs. 2.3, 2.4, 2.5 and 2.6, the elastic modulus E can be related to P_{max}, h_{max}, and S measured from the nanoindentation P vs. h curve.

In the Continuous Stiffness Measurement (CSM) method, the procedure above is modified by measuring the unloading stiffness dP/dh continuously along the load–displacement nanoindentation curve (P vs h curve). This is accomplished by superimposing a small harmonic oscillating force on top of the normal force vs. time curve obtained by application of the constant indentation rate [32, 34]. The value of S in this case is:

$$S = \frac{dP}{dh} = \left[\frac{1}{\frac{P_{os}}{h(\omega)}\cos\phi - (K_s - m\omega^2)} - K_f^{-1}\right] \tag{2.7}$$

where, P_{os} is the peak value of the applied harmonic force with frequency ω, h(ω) is the magnitude of the indenter displacement when the harmonic force is applied, p is the phase angle between the force and displacement, m is the mass of indenter, K_s is the spring constant of leaf spring supporting indenter, and K_f is stiffness of the indenter [33, 34]. The values of E and H can then be evaluated continuously as a function of the indentation depth h during the nanoindentation test by using Eqs. 2.1, 2.2, 2.3, 2.4, 2.5, and 2.6 and the values of dP/dh, P, h recorded at each point along the nanoindentation curve.

Typical CSM results for the hardness and elastic modulus as a function of indentation depth for a single indent in a SAC305 solder joint are shown in Figs. 2.4 and 2.5, respectively.

The results were found to stabilize and be independent of depth after approximately 1,500 nm of indentation depth. Thus, we have determined the E and H values in this work by finding the average the values of the CSM response curves for

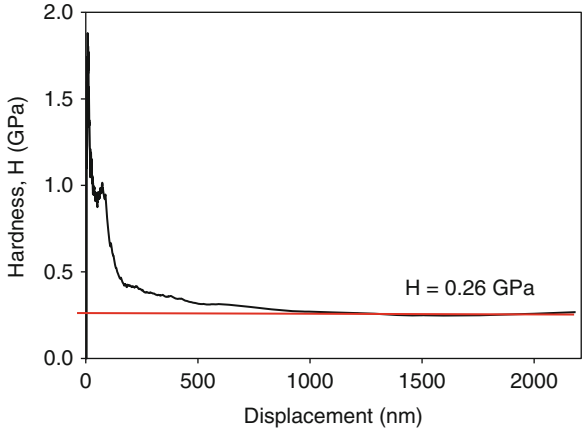

Fig. 2.5 Nanoindentation hardness of SAC305 solder as a function of indentation depth

Property	Joint #1	Joint #2	Joint #3
Elastic Modulus (GPa)	47.10	50.25	55.59
Hardness (GPa)	0.260	0.310	0.340

Fig. 2.6 SAC305 solder ball mechanical properties

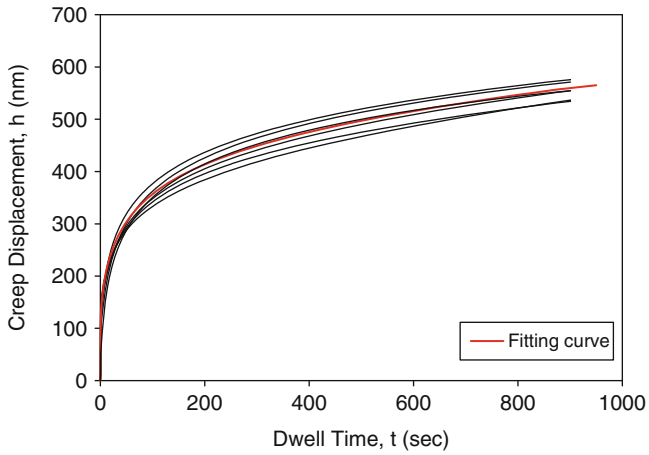

Fig. 2.7 Creep displacement data for SAC305 solder

h > 1,500 nm. For the indentation test data in Figs. 2.4 and 2.5, the extracted values were E = 47.1 GPa and H = 0.26 GPa for this solder joint. Thus, the compressive yield stress can be estimated by σ_Y = H/3 = 86.7 MPa. Values for other joints are tabulated in Fig. 2.6. The variations from joint to joint are due to the anisotropy of the β-Sn matrix of the SAC solder [37–40]

2.3.2 Measurement of Creep Behavior

Nanoindentation creep testing was performed during the hold/dwell at the peak load of 30 mN as shown in Fig. 2.3. Dwell times of 500–1,000 s were considered in this work. The total displacements were measured continuously, and the creep displacement data (change in displacement) during the constant load period were extracted. For example, Fig. 2.7 illustrates the measured creep displacement vs. time response for an array of six indents performed a single solder joint under similar conditions. The creep displacement data can be fit well with a variety of empirical models. In this work, we have chosen to use a log hyperbolic tangent model [41]

$$h = C_1 \ln(1 + t) + C_2 \tanh(C_3 t) + C_4 t + C_5 \tag{2.8}$$

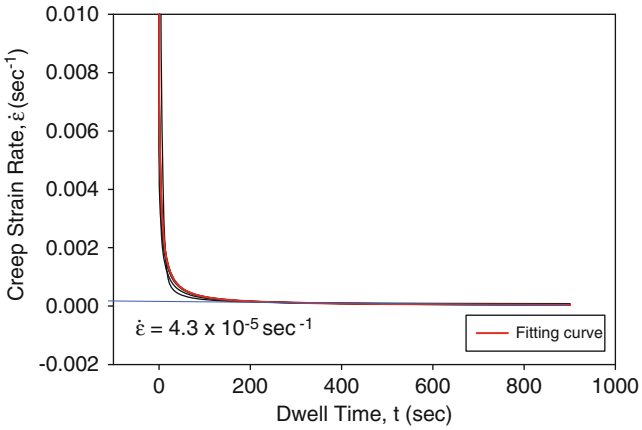

Fig. 2.8 Creep strain rate versus time for SAC305 solder

where C_1, C_2, C_3, C_4 and C_5 are fitting constants. The red curve in Fig. 2.6 is the fit of Eq. 2.8 to the creep data from the six individual indent curves.

The creep rate (creep deformation rate) is determined by taking the derivative of the creep displacement vs. time response:

$$\dot{h} = \frac{dh}{dt} \tag{2.9}$$

Using the fitting curve in Eq. 2.8, the creep rate can be easily evaluated as a function of time. The concept of indentation creep strain rate was developed by Mayo and Nix [42, 43], and is defined by dividing the creep deformation rate by the instantaneous creep deformation at each time:

$$\dot{\varepsilon} = \frac{1}{h}\frac{dh}{dt} \tag{2.10}$$

By again using the fitting curve in Eq. 2.8, the creep rate can be easily evaluated as a function of time. For the creep deformation data in Fig. 2.7, the creep strain rate vs. time response is plotted in Fig. 2.8, and a nearly constant strain rate value of 4.3×10^{-5} s^{-1} was obtained for a long creep time of 900 s.

The nanoindentation creep response never actually achieves a constant strain rate due to the fact that the projected contact area A of the indentation continues to grow during the creep deformation period (constant load region). For example, evolution of the hardness H for the responses in Fig. 2.7 were calculated using the applied constant load of $P_{max} = 30$ mN, and the time evolving contact area calculated from the measured the creep deformations and Eqs. 2.3 and 2.4. Figure 2.9 illustrates the hardness vs. time response for the six individual indents and the fitting curve from Fig. 2.7. Using the Tabor relation in Eq. 2.2, the applied compressive creep stress vs. time can be estimated using $\sigma = H/3$, and Fig. 2.10 shows the stress vs. time response for the individual six individual indents and the fitting curve from Fig. 2.7. It is seen from Figs. 2.9 and 2.10 that the creep stress becomes fairly constant ($\sigma = 54$ MPa) after 900–1,000 s of constant load application. Thus, the asymptotic strain rate extracted from Fig. 2.8 can be estimated to be steady state strain rate for this stress level.

The entire strain rate vs. applied stress response for the SAC305 solder can be estimated by extracting the creep rate from the fitting curve in Fig. 2.8 and the applied stress from the fitting curve in Fig. 2.10 for each time, and then replotting the results to eliminate time as shown in Fig. 2.11. With this approach, a single nanoindentation experiment can be used to generate the complete creep strain rate vs. stress response of the material. The first point on the curve in Fig. 2.11 has the coordinates $\dot{\varepsilon} = 4.3 \times 10^{-5}$ s^{-1} and $\sigma = 54$ MPa, and are the values obtained for the long dwell time of 900 s. Since the nanoindentation tests are compressive in nature, the applied stress levels in Fig. 2.11 ($\sigma > 54$ MPa) possible via nanoindentation are well above those that are normally possible and of interest for lead free solders in tension or shear. For example, the tensile stress levels typically used in tensile creep testing are in the range of 10–30 MPa [2–6]. The low stress creep response can be extrapolated from the nanoindentation measured compressive creep response by nonlinear regression fitting of the data in Fig. 2.11 using one of the popular creep models for lead free solders such as the exponential model

$$\dot{\varepsilon} = C_1 e^{C_2 \sigma} \tag{2.11}$$

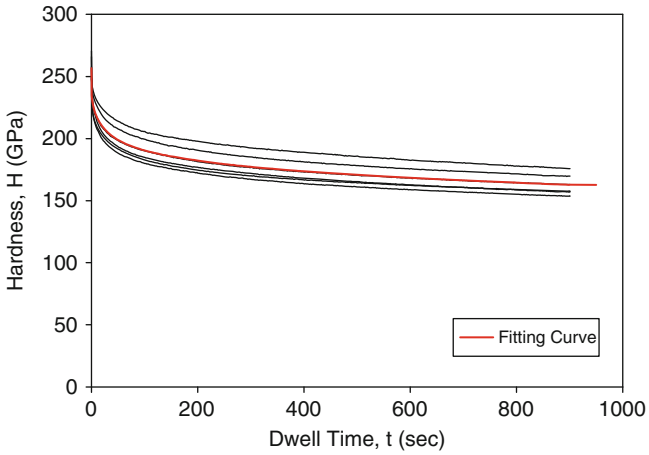

Fig. 2.9 Hardness versus time for SAC305 solder during the nanoindentation creep loading

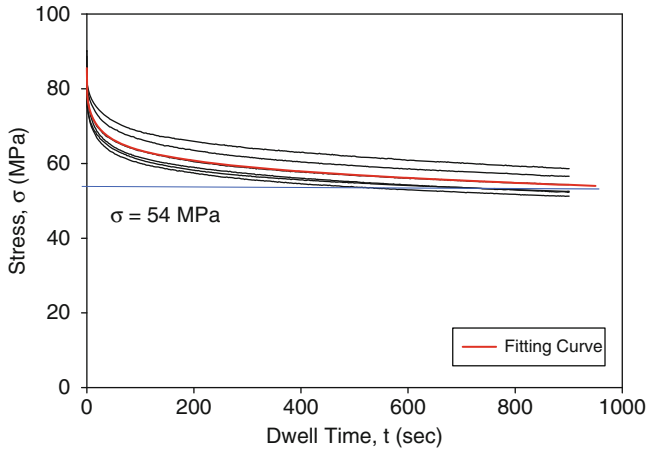

Fig. 2.10 Stress versus time for SAC305 solder during the nanoindentation creep loading

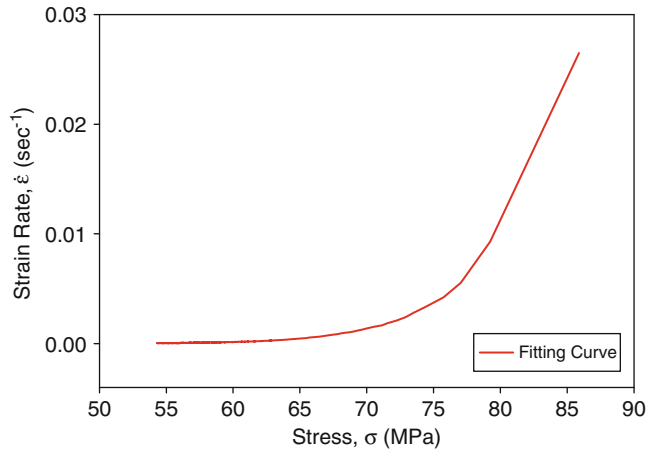

Fig. 2.11 Creep strain rate versus stress for SAC305 solder extracted from the nanoindentation creep data

or the Garofalo model

$$\dot{\varepsilon} = C_1[\sinh(C_2\sigma)]^{C_3}e^{-C_4/T} \tag{2.12}$$

where the C_i ($i = 1, 2, 3, 4$) are fitting constants. These calculations have performed and the results are illustrated in the log-log plots in Figs. 2.12 and 2.13. In each of these graphs, the red curve is the measured nanoindentation creep response

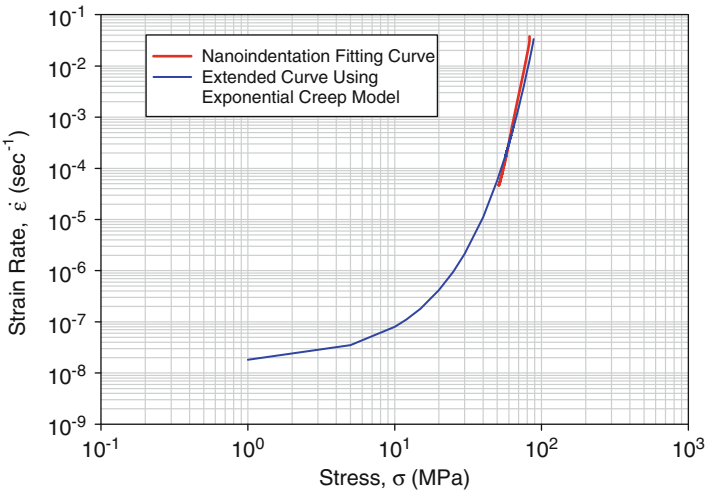

Fig. 2.12 Creep strain rate versus stress for SAC305 solder using the exponential creep model

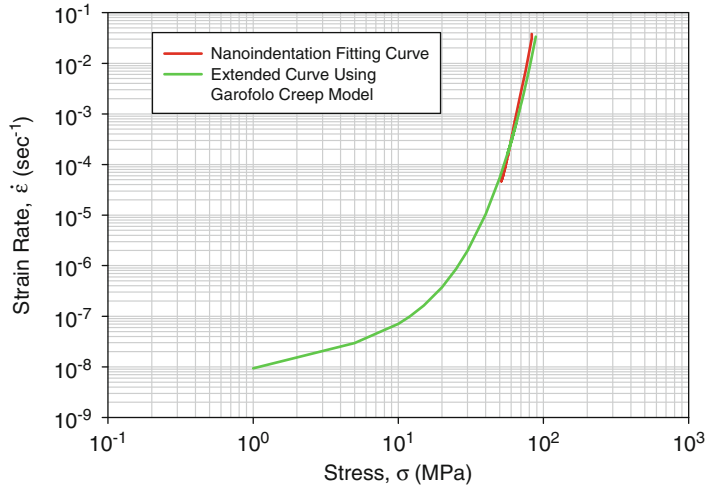

Fig. 2.13 Creep strain rate versus stress for SAC305 solder using the Garofalo creep model

from Fig. 2.10, while the blue and green curves are the regression fitting results using the exponential and Garofalo models, respectively. Both creep models are able to fit the nanoindentation creep results equally well, and both give nearly the same results when extrapolated to lower stress levels.

2.4 Summary and Conclusions

In the current paper, the mechanical properties and creep behavior of lead free solders have been characterized by nano-mechanical testing of single SAC305 solder joints extracted from PBGA assemblies. Using nanoindentation techniques, the stress–strain and creep behavior of the SAC solder materials have been explored at the joint scale. Mechanical properties characterized included the elastic modulus, hardness, and yield stress. The test results show that the mechanical properties (modulus, hardness) of single grain SAC305 joints were dependent on the crystal orientation. Using a constant force at max indentation, the creep response of the solder joint materials has also been measured as a function of the applied stress level. An approach has been developed to estimate tensile creep strain rates for low stress levels using nanoindentation creep data measured at very high compressive stress levels.

Acknowledgments This work was supported by Center for Advanced Vehicle Electronics and Extreme Environment (CAVE^3). We thank the members of iNEMI for providing the joint samples tested in this work.

References

1. Ma H, Suhling JC (2009) A review of mechanical properties of lead-free solders for electronic packaging. J Mater Sci 44:1141–1158
2. Ma H, Suhling JC, Lall P, Bozack MJ (2006) Reliability of the aging lead-free solder joint. In: Proceedings of the 56th electronic components and technology conference, San Diego, pp 849–864
3. Ma H, Suhling JC, Zhang Y, Lall P, Bozack MJ (2007) The influence of elevated temperature aging on reliability of lead free solder joints. In: Proceedings of the 57th IEEE electronic components and technology conference, Reno, pp 653–668
4. Zhang Y, Cai Z, Suhling JC, Lall P, Bozack MJ (2008) The effects of aging temperature on SAC solder joint material behavior and reliability. In: Proceedings of the 58th IEEE electronic components and technology conference, Orlando, pp 99–112
5. Zhang Y, Cai Z, Suhling JC, Lall P, Bozack MJ (2009) The effects of SAC alloy composition on aging resistance and reliability. In: Proceedings of the 59th IEEE electronic components and technology conference, San Diego, pp 370–389
6. Cai Z, Zhang Y, Suhling JC, Lall P, Johnson RW, Bozack MJ (2010) Reduction of lead free solder aging effects using doped SAC alloys. In: Proceedings of the 60th electronic components and technology conference, Las Vegas, pp 1493–1511
7. Mustafa M, Cai Z, Suhling J, Lall P (2011) The effects of aging on the cyclic stress–strain behavior and hysteresis loop evolution of lead free solders. In: Proceedings of the 61st electronic components and technology conference, Orlando, pp 927–939
8. Motalab M, Cai Z, Suhling JC, Zhang J, Evans JL, Bozack MJ, Lall P (2012) Improved predictions of lead free solder joint reliability that include aging effects. In: Proceedings of 62nd electronic components and technology conference, San Diego, pp 513–531
9. Zhang J, Thirugnanasambandam S, Evans JL, Bozack MJ, Zhang Y, Suhling JC (2012) Correlation of aging effects on the creep rate and reliability in lead free solder joints. SMTA J 25(3):19–28
10. Pang JHL, Low TH, Xiong BS, Xu L, Neo CC (2004) Thermal cycling aging effects on Sn–Ag–Cu solder joint microstructure, IMC and strength. Thin Solid Films 462–463:370–375
11. Darveaux R (2005) Shear deformation of lead free solder joints. In: Proceedings of the 55th IEEE electronic components and technology conference, Lake Buena Vista, FL, pp 882–893
12. Wiese S, Wolter KJ (2007) Creep of thermally aged SnAgCu solder joints. Microelectron Reliab 47:223–232
13. Dutta I, Pan D, Marks RA, Jadhav SG (2005) Effect of thermo-mechanically induced microstructural coarsening on the evolution of creep response of SnAg-based microelectronic solders. Mater Sci Eng A 410–411:48–52
14. Fischer-Cripps AC (2011) Nanoindentation, 3rd edn. Springer, New York, NY, USA
15. Rhee H, Lucas JP, Subramanian KN (2002) Micromechanical characterization of thermo-mechanically fatigued lead-free solder joints. J Mater Sci Mater Electron 13:477–484
16. Lucas JP, Rhee H, Guo F, Subramanian KN (2003) Mechanical properties of intermetallic compounds associated with Pb-free solder joints using nanoindentation. J Electron Mater 32(12):1375–1383
17. Chromik RR, Vinci RP, Allen SL, Notis MR (2003) Measuring the mechanical properties of lead free solder and Sn-based intermetallics by nanoindentation. J Met 55(6):66–69
18. Deng X, Chawla N, Chawla KK, Koopman M (2004) Deformation behavior of (Cu, Ag)-Sn intemetallics by nanoindentation. Acta Mater 52:4291–4303
19. Deng X, Chawla N, Chawla KK, Koopman M (2004) Young modulus of (Cu, Ag)-Sn intemetallics by nanoindentation. Mater Sci Eng A 364:240–243
20. Gao F, Taekmoto T (2006) Mechanical properties evolution of Sn-3.5Ag based lead free solders by nanoindentation. Mater Lett 60:2315–2318
21. Gao F, Nishikawa H, Takemoto T (2007) Nanoscale mechanical response of Sn-Ag based lead free solders. In: Proceedings of the IEEE electronic components and technology conference, Reno, NV, pp 206–210
22. Sun Y, Liang J, Xu JH, Wang G, Li X (2008) Nanoindentation for measuring individual phase mechanical properties of lead free solder alloy. J Mater Sci Mater Electron 19:514–521
23. Liu YC, Teo JWR, Tung SK, Lam KH (2008) High temperature creep and hardness of eutectic 80Au/20Sn solder. J Alloys Compd 448:340–343
24. Gao F, Nishikawa H, Takemoto T, Qu J (2009) Mechanical properties versus temperature relation of individual phase in Sn-3.0Ag-0.5Cu lead free solder alloy. Microelectron Reliab 49:296–302
25. Han YD, Jing HY, Nai SML, Xu LY, Tan CM, Wei J (2010) Indentation size effect on the creep behavior of SnAgCu solder. Int J Mod Phys B 24(1–2):267–275
26. Han YD, Jing HY, Nai SML, Xu LY, Tan CM, Wei J (2010) Temperature dependence of creep and hardness of Sn-Ag-Cu lead free solders. J Electron Mater 39(2):223–229
27. Xu L, Pang JHL (2006) Nanoindentation on SnAgCu solder joints and analysis. J Electron Mater 35(12):2107–2115
28. Xu L, Pang JHL (2006) Nanoindentation characterization of Ni-Cu-Sn IMC layer subjected to isothermal aging. Thin Solid Films 504:362–366
29. Song JM, Huang BR, Liu CY, Lai YS, Chiu YT, Huang TW (2012) Nanomechanical response of intermetallic phase at the solder joint interface-crystal orientation and metallurgical effects. Mater Sci Eng A 534:53–59
30. Venkatadri V, Yin L, Xing Y, Cotts E, Srihari K, Borgesen P (2009) Accelerating the effects of aging on reliability of lead free solder joints in a quantitative fashion. In: Proceedings of the IEEE electronic components and technology conference, San Diego, CA, pp 398–405
31. Henshall G (2009) iNEMI lead-free alloy alternatives project report: thermal fatigue experiments and alloy test requirements. In: Proceedings of the SMTAI, San Diego, CA, pp 317–324
32. Pharr GM, Oliver WC, Brotzen FR (1992) On the generality of the relationship among contact stiffness, contact area, and elastic modulus during indentation. J Mater Res 7(3):613–617
33. Oliver WC, Pharr GM (1992) An improved technique for determining hardness and elastic modulus using load and displacement sensing indentation experiments. J Mater Res 7(6):1564–1583
34. Hay J, Agee P, Herbert E (2010) Continuous stiffness measurement during instrumented indentation testing. Exp Tech 34(3):86–94
35. Tabor D (1951) Hardness of metals. Oxford University Press, Oxford, UK
36. Zhang P, Li SX, Zhang ZF (2011) General relationship between strength and hardness. Mater Sci Eng A 529:62–73

37. Lee BZ, Lee DN (1998) Spontaneous growth mechanism of tin whiskers. Acta Mater 46(10):3701–3714
38. Bieler TR, Jiang H, Lehman LP, Kirkpatrick T, Cotts EJ, Nandagopal B (2008) Influence of Sn grain size and orientation in the thermomechanical response and reliability of Pb-free solder joints. IEEE Trans Compon Pack Technol 31(2):370–381
39. Telang TU, Bieler TR (2005) The orientation imaging microscopy of lead free Sn-Ag solder joints. J Met 57(6):44–49
40. Yang S, Tian Y, Wang C (2010) Investigation on Sn grain number and crystal orientation in the Sn-Ag-Cu/Cu solder joints of different sizes. J Mater Sci Mater Electron 21:1174–1180
41. Chhanda N, Suhling JC, Lall P (2011) Experimental characterization and viscoplastic modeling of the temperature dependent material behavior of underfill encapsulants. In: Proceedings of InterPACK 2011, ASME, Paper no. IPACK2011-52209, pp 1–13
42. Mayo MJ, Nix WD (1988) A micro-indentation study of superplasticity in Pb, Sn and Sn-38 wt%Pb. Acta Mater 36(8):2183–2192
43. Mayo MJ, Nix WD (1990) Mechanical properties of nanophase TiO2 as determined by nanoindentation. J Mater Res 5(5):1073–1082

Springer

http://www.springer.com/978-3-319-00779-3

MEMS and Nanotechnology, Volume 5
Proceedings of the 2013 Annual Conference on
Experimental and Applied Mechanics
Shaw III, G.; Prorok, B.C.; Starman, L.; Furlong, C. (Eds.)
2014, VIII, 134 p. 124 illus., Hardcover
ISBN: 978-3-319-00779-3